

Article

On the Origin of Bastnaesite-(La,Nd,Y) in the Nissi (Patitira) Bauxite Laterite Deposit, Lokris, Greece

Sofia Kalatha ¹, Maria Perraki ^{2,*}, Maria Economou-Eliopoulos ¹ and Ioannis Mitsis ¹

¹ Faculty of Geology & Geoenvironment, National and Kapodistrian University of Athens, University Campus Zografou, GR-15784 Athens, Greece; spkalatha@gmail.com (S.K.); econom@geol.uoa.gr (M.E.-E.); mitsis@geol.uoa.gr (I.M.)

² School of Mining & Metallurgical Engineering, National Technical University of Athens, 9 Heroon Politechniou St., GR-15773 Zografou, Athens, Greece

* Correspondence: maria@metal.ntua.gr; Tel.: +30-210-772-2115

Academic Editors: Juan Diego Rodriguez-Blanco and Adrian Jones

Received: 23 November 2016; Accepted: 14 March 2017; Published: 21 March 2017

Abstract: A detailed geochemical study and a thorough mineralogical description of the rare-earth elements (REE)-minerals and associated minerals were carried out in two vertical profiles of approximately 4 m length, from the Nissi (Patitira) bauxite laterite deposit, Lokris, Greece, characterized by the presence of goethite in small sizes resembling bacterial cell coated by goethite and a significant REE enrichment. The enrichment of the REE concentrated in bastnaesite-group minerals, the intergrowths between REE-minerals and Al–Ni–silicates with significant sulfur contents and their association with goethite microtextures interpreted as bacteriomorphic, indicate REE remobilization along with iron bio-leaching and re-precipitation on karstified limestone. In addition to the previous-reported hydroxylbastnaesites, a (La,Nd,Y)(CO₃)F member of the bastnaesite-group associated with Al–Ni–silicates were identified, the stability of which may reflect the dependence on the source rocks and the local variations of pH-Eh. Interaction between downward percolating water and carbonate rocks seems to be a very effective mechanism for REE fluorocarbonates deposition under alkaline and reducing conditions.

Keywords: rare-earth elements (REE); bastnaesite; karstic Fe–Ni–laterites; bauxite laterites; Lokris; Greece

1. Introduction

The Fe–Ni laterite deposits in Greece are a major source of nickel, a metal of strategic significance. Greece’s Fe–Ni ore reserves are currently estimated to be in the range of 200 Mt at 0.9%–1.4% Ni ([1] and references therein). Aghios Ioannis mining area includes Nissi area deposits (located SSW of the Aghios Ioannis deposit) (Figure 1; [2]). The laterite ores at Aghios Ioannis and Nissi area deposits have been eroded, transported, and deposited onto karstified Triassic–Jurassic limestones and are conformably overlain by Upper Cretaceous limestones (Figure 1). The Nissi area deposits are comprised of a series of lenses, that may occur either as isolated typical Fe–Ni–laterite or bauxite laterite ores or as an association of Fe–Ni ore at the lowest part of the deposit, followed by bauxite laterite towards its upper part ([3] and references therein)—such as the Patitira deposit (located at the eastern part of the Nissi area) (Figure 1).

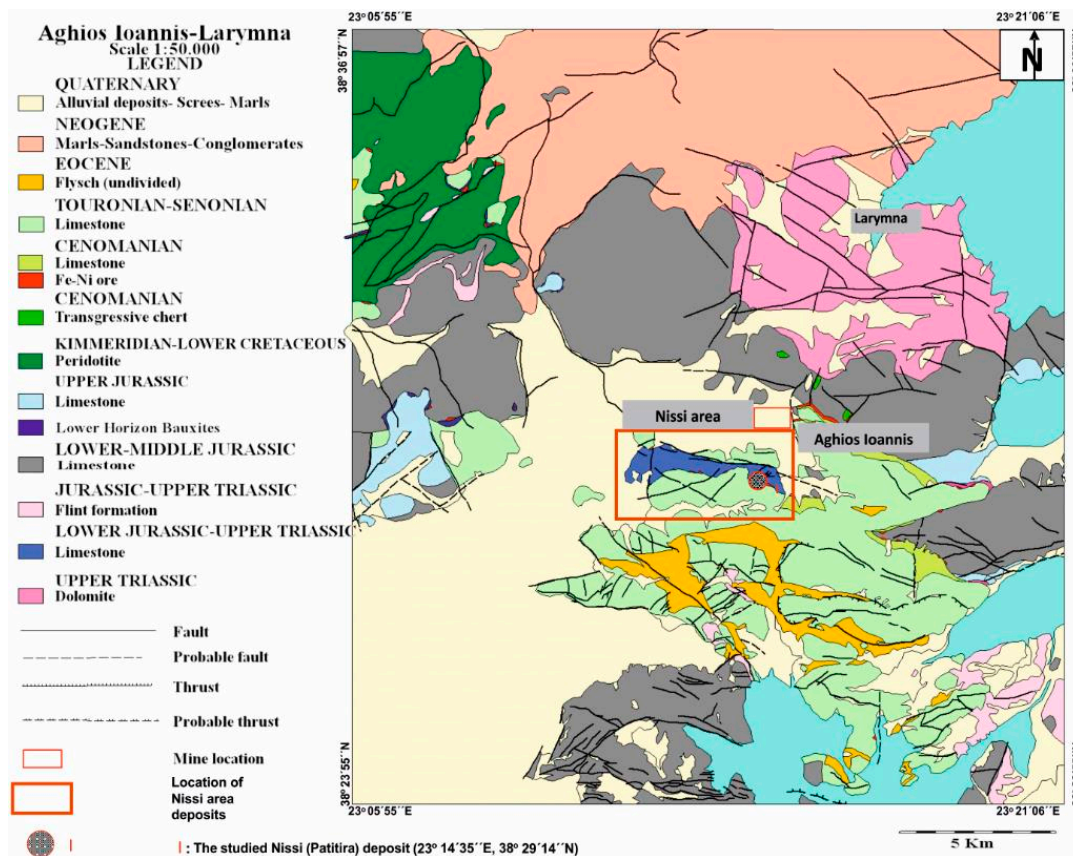


Figure 1. Simplified geological map, after GMM LARCO SA, cited in ProMine Project [2] showing the location of the studied deposit in Lokris area, Greece. The position of the sampled profiles is marked by the red cycle.

Geochemical characteristics of the Ni-laterite deposits in Lokris have been studied for major and trace elements, including rare earth elements and chemistry of minerals in those deposits [1,3–9]. At the Nissi deposits, a strong enrichment of light rare-earth elements (LREE) relative to heavy rare-earth elements (HREE), due to the presence of the authigenic hydroxylbastnaesite-(Nd) minerals, has already been described [8,10]. Nickel-bearing minerals, such as takovite, Mn–Co–Ni asbolane, hydrated halloysite and an unknown Al–Ni–silicate from the Aghios Ioannis deposit have been described [1,11–14].

Present study focuses on two vertical profiles from the Nissi (Patitira) bauxite laterite deposit, in Lokris area, characterized by the presence of goethite microtextures resembling a bacteriomorphic mineral (Profile I) and significant REE enrichment (Profile II). Geochemical variations and a detailed description of the REE-minerals and associated minerals are given in an attempt to define the factors controlling the compositional variation in REE minerals and the REE concentration process.

2. Geological Setting

Nickel laterites in Central Greece formed as Early Cretaceous [4–8,15] by prolonged and intense weathering of ultramafic rocks [1] and may have been partially preserved in situ or transported, re-deposited as marine sediments (mixed, in some cases, with weathering material derived from non-ultramafic protoliths) and buried by later sedimentary rocks ([1] and references therein). Evidence of the allochthonous origin of the Aghios Ioannis–Nissi deposits through repeated marine transgression and regression with associated re-working and deposition in a shallow marine environment as well as diagenetic and post-diagenetic processes have been documented in previous works [1,4–8,13].

All of these deposits are allochthonous, lie on karstified Triassic–Jurassic limestones, are conformably overlain by Upper Cretaceous limestones and have been affected by faulting [4–14,16]. The contacts between ore and the overlain Cretaceous and underlain Triassic–Jurassic limestones are irregular, whereas irregular bodies of Cretaceous limestones are enclosed within Fe–Ni–laterite ore. The Nissi deposits are overlain by a sequence of mudstone, limestones and organic carbon-rich mudstones, which has been attributed to stagnant reducing marine environment during tectonic down warping [6]. In addition, the occurrence of low to moderate porosity limestone resembling travertine limestone may be indicative of a shallow water environment close to the continental shore [17].

A peculiarity of the Nissi (Patitira) deposit lying on Triassic–Jurassic limestone is the association of bauxite laterite ore towards its upper part, with Ni-rich bauxite laterite ore characterized by an epigenetic enrichment in Ni,Co,Mn (asbolane), Al–Ni–silicates and REE at the lowest part of the deposit, close to its contact with the basement limestone, and within limestone itself (Figures 2 and 3; [3,6,9,18]). In addition, the upper transition zone between Cretaceous limestone and the Nissi laterite deposit is characterized by an association of framboidal pyrite with organic matter; the zone below the laterite ore and the carbonate basement is characterized by the occurrence of bacteriomorphic goethite [16].

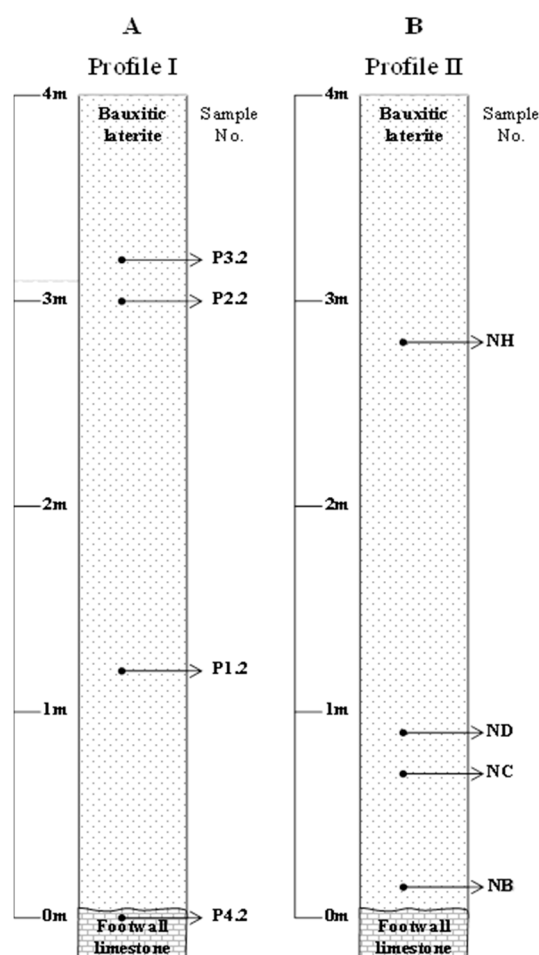


Figure 2. The columnar sections of the studied bauxite laterite profiles at Patitira (Figure 1, red cycle).

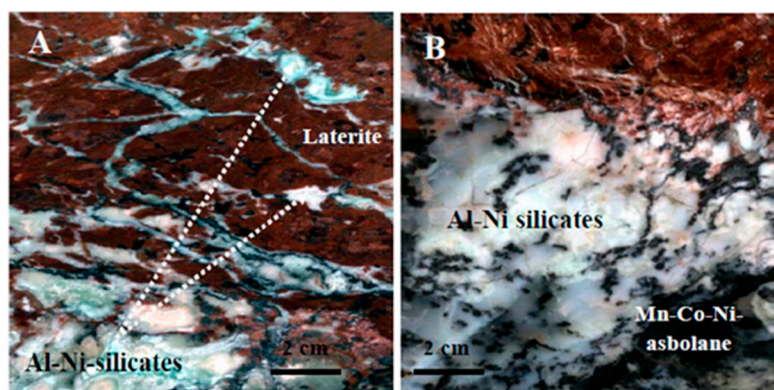


Figure 3. Photographs showing the re-deposition of epigenetic Al–Ni–silicates (A,B) and Mn–Co–Ni asholane (B) at the contact between the bauxite laterite ore and the carbonate basement from the Patitira (Figures 1 and 2, Profile II).

3. Methods of Investigation

In order to identify geochemical trends from the overlying limestone to the footwall limestone, sampling along two relatively small vertical laterite profiles (Profile I and Profile II), covering the exposed area of the Patitira deposit (Figures 1 and 2), was carried out. Eight samples weighing about 3 kg each were selected (out of 20 collected) as representative ores. Their stratigraphic position and description are given in Table 1. Polished sections of all samples were examined using reflected light microscope, scanning electron microscope (SEM), equipped with energy dispersive spectroscopy (EDS). The SEM-EDS analyses were carried out at the Faculty of Geology and Geoenvironment, National and Kapodistrian University of Athens (NKUA), using a JEOL JSM 5600 scanning electron microscope (Tokyo, Japan), equipped with ISIS 300 OXFORD automated energy dispersive analysis system (Oxfordshire, UK). Analytical conditions were 20 kV accelerating voltage, 0.5 nA beam current, <math><2\ \mu\text{m}</math> beam diameter and 50 s count times. The following X-ray lines were used: AsLa, FeKa, NiKa, CoKa, CuKa, CrKa, AlKa, TiKa, CaKa, SiKa, MnKa, MgKa, ClKa, LaLa, CeLa, PrLa, NdLa, GdLa, and YLa. Pure metals standards were used for Cu, Ni, Co and Cr, and pyrite for S and Fe. Standard indium arsenide and 300 s counting time were used for As and the presence of arsenic was confirmed by the X-ray spectrum. Careful calibration for REE was carried out using LaB₆ for La, CeO₂ for Ce, PrF₃ for Pr, NdF₃ for Nd, GdF₃ for Gd and Y. In addition to the above carbon coated samples, a few polished sections showing unpolished parts, revealing the presence of goethite micro-textures resembling bacterial cell were coated by gold and analyzed, in order to identify traces of carbon and other components of organic material.

Major and trace elements in laterite samples were determined by ICP–MS analysis, at the XRAL Laboratories Ltd., Ancaster, ON, Canada. Detection limits are 0.1 ppm for Ni and Co and all analyzed rare earth elements, 0.5 ppm for As, 1 ppm for Cr and Mn, 0.01 wt % for Fe, Ca, Mg, and Al, 0.05 wt % for S, and 0.001 wt % for Ti. According to the results for the quality control samples, the precision of the analyses of the minor and trace elements is in good agreement with international standards.

The samples were dissolved using a strong multi-acid (HNO₃–HClO₄–HF) digestion and the residues dissolved in concentrated HCl. The moisture content was determined by drying the samples at 105 °C and the organic matter content was determined by igniting the oven-dried samples (from moisture content determination) in a muffle furnace at 440 °C for 3 h [19] and calculating the weight difference as a percentage (NKUA).

Table 1. List of samples, stratigraphic position, description and their mineralogical composition.

Patitira Profile I			
Sample	Altitude (m)	Description	Minerals
P3.2	3.2	Bauxite Laterite	Bhm, Gth, Hem, Chl, Qz, Ti-oxides
P2.2	3	Bauxite Laterite	Gth, Bhm, Hem, Chr, Chl, Ti-oxides
P1.2	1.2	Ni-rich Bauxite Laterite	Bacterio-morphic Gth, Ilt, Ti-oxides, Chr, Hem, Qz
P4.2	0	Footwall Limestone	Cal, Mn-oxides (in veinlets)
Patitira Profile II			
Sample	Altitude (m)	Description	Minerals
NH	2.8	Bauxite Laterite	Bhm, Gbs, Gth, Chl, Qz, Kln, Chr, Hem, Ti-oxides
ND	0.9	Ni-rich Bauxite Laterite	Gth, Hem, Chl, Ilt, Qz, Cal, Chr, Kln, Bhm, Ti-oxides
NC	0.7	Ni-rich Bauxite laterite	Gth, Hem, Chl, Ilt, Qz, Cal, Chr, Kln, Bhm, Ti-oxides
NB	0.15	Ni-rich Bauxite Laterite	Gbs, Hal, Lz, REE minerals (Bas), Gth, Tak, UM, Chl, Ilt, Kln, Mnt, Sme, Cal, Asb, Ti-oxides

Symbols: Asb = asbolane, Bas = bastnaesite, Bhm = boehmite, Cal = calcite, Chl = chlorite, Chr = chromite, Gbs = gibbsite, Gth = goethite, Hal = halloysite, Hem = hematite, Ilt = illite, Kln = kaolinite, Lz = lizardite, Mnt = montmorillonite, Sme = smectite, REE = Rare Earth Elements, Tak = takovite, Qz = quartz, UM = unknown Ni-Al hydrosilicate.

X-ray powder diffraction (XRD) data were obtained using a Siemens Model 5005 X-ray diffractometer (Bruker AXS GmbH., Karlsruhe, Germany), Cu K α radiation at 40 kV, 40 nA, 0.020° step size and 1.0 s. step time. The XRD patterns were evaluated using the EVA 10.0 program of the Siemens DIFFRAC (Bruker AXS GmbH.) and the D5005 software package (NKUA).

Raman spectra were recorded with a Renishaw RM1000[®] Raman micro-spectrometer (Renishaw, UK) at the School of Mining and Metallurgical Engineering of the Technical University of Athens, Greece. Spectra were excited at room temperature with the 632.8 nm line of a red 19 mW He-Ne laser through an OLYMPUS[®] $\times 100$ objective (Olympus Co., Tokyo, Japan). Each unpolarized spectrum represents the accumulation of three acquisitions of 20 s each. The spectra were collected at a constant laboratory temperature (20 °C) with a Peltier-cooled charge coupled device (CCD) detector, and the positions of the Raman bands were controlled and eventually corrected by regularly measuring the position of the Rayleigh line. The spectral resolution was about 0.4 cm⁻¹. The numerical aperture of the objective was 0.9. The laser spot on the surface had a diameter of approximately 1 μ m and a power of 4 mW. The entrance slit into the spectrometer was set to 40 μ m. Light was dispersed by a holographic grating with 1800 grooves/mm. No baseline correction was performed to the spectra. Spectra were treated with the GRAMS32 software (Version 7.0, Galactic Industries Corp., Salem, NH, USA).

4. Geochemical Characteristics

The geochemical results (Tables 2 and 3) of representative samples (Table 1) from the Nissi (Patitira) deposit show a wide variation in major, minor and trace elements, which appear to be consistent with their mineralogical composition. There is a significant variation in the Al₂O₃ content ranging from 19.1 wt % in the Ni-rich bauxite laterite up to 44 wt % in the bauxite laterite. The highest MnO (0.66 wt %) and NiO (6.33 wt %) contents were found in the group of Ni-rich samples labeled as NB (NB value is the average value of five samples) from the contact between the lowermost part of bauxite laterite body and the contact with footwall limestone. The significant arsenic content and its association with goethite that is a major component in bauxite laterites have been well documented (Table 2). The investigation of all samples revealed the presence of significant organic content, ranging from 1.26 wt % to 7.8 wt % organic matter (O.M.) at Profile I (Table 2) and from 1.1 wt % to 5.2 wt % O.M. at Profile II (Table 3).

Table 2. Chemical composition of the bauxite laterites from the Patitira Profile I. O.M.: organic matter; L.O.I.: Loss on ignition; n.d.: not detected.

Weight Percentage (wt %)	Ni-Rich Bauxite Laterite (Sample P1.2)	Bauxite Laterite (Sample P2.2)	Bauxite Laterite (Sample P3.2)	Footwall Limestone (Sample P4.2)
SiO ₂	16.23	12.78	13.82	2.40
Fe ₂ O _{3total}	44.61	54.33	49.62	0.11
Al ₂ O ₃	20.61	20.58	22.67	2.50
MgO	0.71	0.88	0.29	0.17
CaO	0.30	0.17	0.26	50.80
TiO ₂	0.76	1.21	1.45	0.01
MnO	0.03	0.41	0.08	0.30
NiO	1.57	0.56	0.13	n.d.
P ₂ O ₅	0.05	0.02	0.05	n.d.
K ₂ O	0.29	n.d.	n.d.	n.d.
Na ₂ O	0.03	n.d.	n.d.	n.d.
SO ₃	n.d.	n.d.	n.d.	0.08
O.M.	4.56	1.26	7.80	0.19
L.O.I.	13.61	7.50	10.65	42.90
Total	98.80	98.44	99.02	
Element Content (ppm)	Ni-Rich Bauxite Laterite (Sample P1.2)	Bauxite Laterite (Sample P2.2)	Bauxite Laterite (Sample P3.2)	Footwall Limestone (Sample P4.2)
Cr	4540	7400	5330	n.d.
Co	240	600	64	680
As	350	340	220	14
La	164	110	22	17
Ce	84	220	80	n.d.
Y	240	61	17	n.d.
(La + Ce)/Y	1.03	5.41	6.00	-
La/Ce	1.95	0.50	0.28	-

Table 3. Chemical composition of the bauxite laterites from the Patitira Profile II.

Weight Percentage (wt %)	Ni-Rich Bauxite Laterite (Sample NB)	Ni-Rich Bauxite Laterite (Sample NC)	Ni-Rich Bauxite Laterite (Sample ND)	Bauxite Laterite (Sample NH)
SiO ₂	17.81	23.51	24.10	1.85
Fe ₂ O ₃	21.35	35.62	35.60	41.60
Al ₂ O ₃	28.46	19.1	20.30	44.00
MgO	1.23	3.46	3.65	0.25
CaO	1.78	0.41	0.20	0.15
TiO ₂	0.34	1.27	1.10	2.70
MnO	0.66	0.10	0.30	0.17
NiO	6.33	3.60	3.50	0.19
O.M.	5.20	3.20	2.1	1.10
L.O.I.	20.98	11.65	9.75	8.95
Total	98.94	98.72	98.50	99.86
Element Content (ppm)	Ni-Rich Bauxite Laterite (Sample NB)	Ni-Rich Bauxite Laterite (Sample NC)	Ni-Rich Bauxite Laterite (Sample ND)	Bauxite Laterite (Sample NH)
Cr	2470	15,100	12,000	5500
Co	2120	430	2200	57
As	682	200	140	230
La	2366	172	144	56
Ce	318	84	126	207
Nd	2014	160	110	50
Sm	351	34	24	3.60
Eu	82	9.20	6.50	1.20
Tb	34	4.90	4.00	0.50
Yb	26	14.10	20.50	3.70
Lu	4	2.16	3.31	0.86
REE _{total}	5195	480	438	323
La/Ce	7.44	2.05	1.14	0.27

Ni-rich bauxite laterite samples (NB) from the contact between the ore and the underlain limestone exhibit a significant enrichment in REE, especially in La (up to 2370 ppm) and Nd (2010 ppm). Average REE_{total} is 5200 ppm. In addition, the shale normalized REE-patterns of these samples exhibit a negative slope and La/Ce > 1 (Figure 4 (left); Tables 2 and 3). They are similar to those of Ni-rich bauxite laterite samples NC and ND, in terms of the La/Ce > 1, whereas the bauxite laterite (NH) shows

La/Ce < 1 (Table 3). These REE patterns for the Ni-rich bauxite laterite samples along the Patitira vertical profile II are comparable to those throughout the Nissi typical Ni-laterite (average) (Figure 4 (right)).

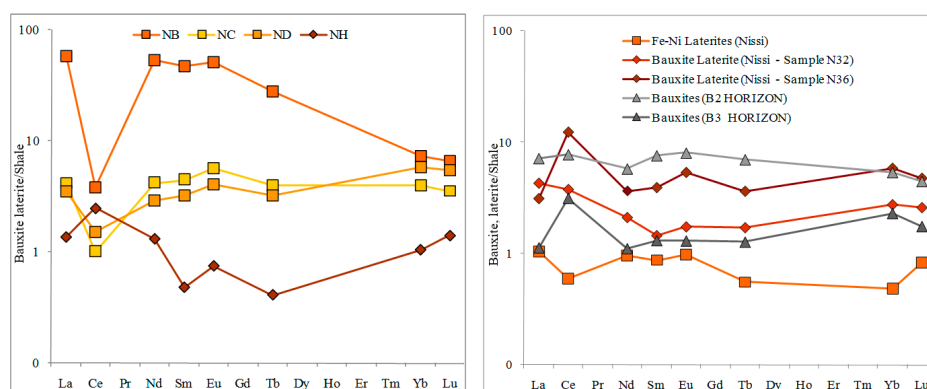


Figure 4. Shale normalized rare-earth elements (REE)-patterns (after Piper, 1974) of Fe–Ni Laterite and Bauxite Laterite ores from the Nissi–Patitira deposits and bauxite ores from the Horizons B2 and B3 of the Parnassos–Ghiona deposits. Data from Table 3; [9,20].

5. Mineralogical Characteristics

Samples collected from the Patitira Profile I (Figure 2A; Table 1) are mostly composed of goethite, limonite, hematite, chromite, boehmite and gibbsite, calcite, Fe-chlorite (chamosite), Ni-bearing chlorite, Ti-oxides and quartz. Angular and/or rounded fragments of goethite often martitized, contain detrital grains of quartz, chromite and chlorite (Figure 5A,B; Table 4). Gibbsite, illite, kaolinite, montmorillonite and Mn–Co–Ni asbolane are abundant towards fractures and the lowest parts of the deposit. The chromite grains or fragments are residual components inherited from the ophiolitic parent rocks of a wide compositional variation, including high-Cr and high-Al types. The most salient feature is the presence of goethite in small sizes resembling bacterial cell coated by goethite (Figure 5C–F; Table 4) ([16] and references therein). In addition, the SEM-EDS study of gold-coated samples (Figure 5F) showed the presence of C, N, Fe, Al, K, Si, Ca, Mn and Ni. Although quantitative analyses were not obtained, due to unpolished surface and the small size of the analyzed material, the presence of the above components may reflect the presence of microorganisms.

Samples labeled as NC and ND, upward in the profile II (Figure 2B; Table 1) consist mainly of goethite, hematite, chlorite, illite, quartz, calcite, chromite, kaolinite, boehmite, and Ti-oxides, whereas the sample labeled as NH consisting mainly of boehmite, gibbsite, goethite, chlorite, quartz, kaolinite, chromite, hematite and Ti-oxides. There is an abundance of gibbsite, illite, kaolinite, montmorillonite, smectite, takovite, Mn–Co–Ni asbolane, halloysite and Al–Ni–Co–Mn silicates towards fractures and the lowest parts of the deposit (Figure 2B).

The XRD pattern (Figure 6) shows the presence of gibbsite, halloysite, lizardite, bastnaesite, goethite, takovite and six reflections recorded at 11.8 Å, 5.90 Å, 3.94 Å, 2.575 Å, 2.443 Å, and 1.503 Å, matching the reflections of an “unknown Al–Ni–silicate mineral” already described by Maksimovic [11,12]. It is notable that this “unknown Al–Ni–silicate mineral” has been described in the localities of Ba and Takovo in Serbia in association with takovite, gibbsite and halloysite and in the karstic nickel deposit of Aghios Ioannis in Lokris area with hydrated halloysite [11,12].

Besides, the XRD pattern shows reflections assigned to any of the following minerals: bastnaesite–La [La(CO₃)F], bastnaesite–Ce [CeCO₃F] and bastnaesite–(Ce,La) [(Ce,La)CO₃F)], in consistency with the relevant data base of the used evaluation software program (EVA 10.0 diffrac plus). Combined XRD and SEM/EDS data (Figures 6 and 7; Tables 5 and 6) indicated the dominance of a (La,Nd,Y)(CO₃)F member of the bastnaesite group. More specifically, bastnaesite occurs mostly in a closed association with intergrowths between takovite and an unknown Al–Ni–silicate mineral (Figures 6 and 7A–E, Tables 5 and 7) or as rounded crystals at the margins of calcite (Figure 7A–C,F). The Al–Ni–silicates

display commonly acicular or needle-shaped morphology, ranging in length from a few tens of nm to several microns. Intergrowths of takovite–Al–Ni–silicate are commonly found as successive thin (a few to tens of μm) layers, composed of fine fibrous crystals of nm to a few μm (Figure 7D,E).

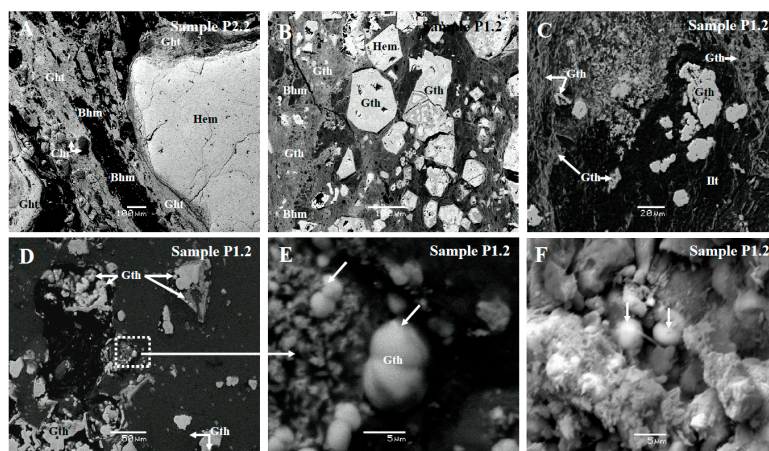


Figure 5. Representative back scattered images of bauxite laterite–Profile I showing: goethite (Gth) with varying composition (Table 4) and different morphological forms: rounded fragments, often martitized (A,B), Fe-(hydroxyl)-oxides pseudomorphs after pyrite (B). The unpolished parts of the sample revealed the presence of goethite micro-textures resembling bacterial cell coated by goethite (white arrows) (C–F).

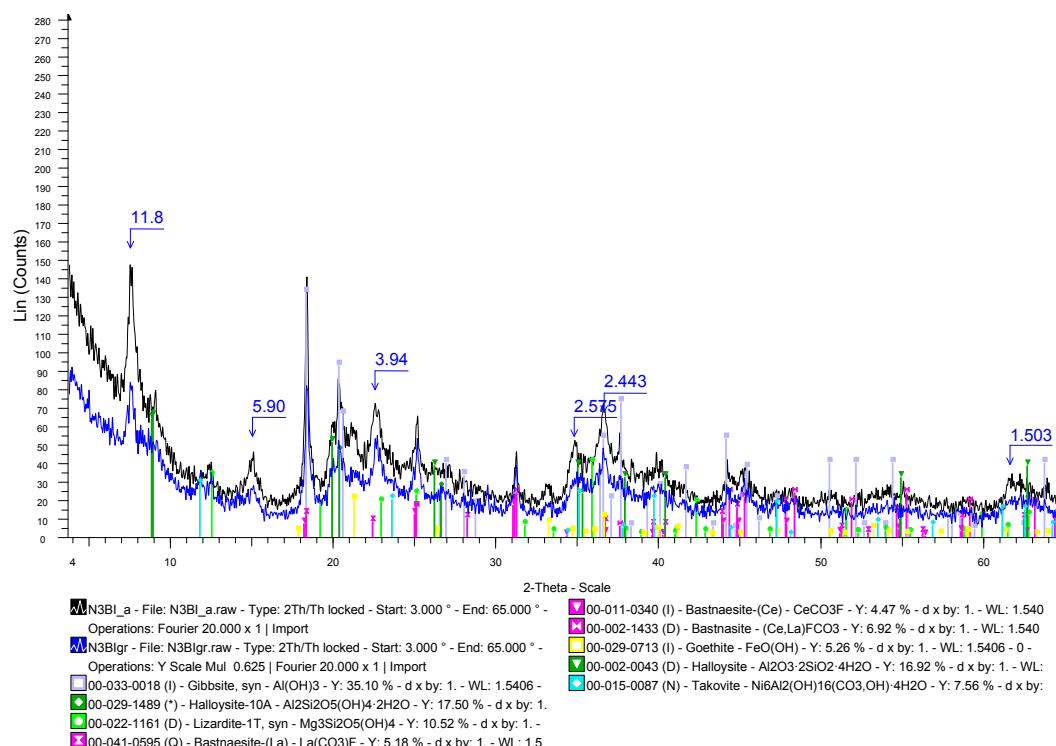


Figure 6. X-ray powder diffraction (XRD) pattern of a Ni-rich bauxite laterite sample (NB group of samples) from the contact between the lowermost part of the bauxite laterite ore and the carbonate basement. Reflections recorded at 11.8 Å, 5.90 Å, 3.94 Å, 2.575 Å, 2.443 Å, and 1.503 Å are attributed to the unknown Al–Ni–silicate mineral.

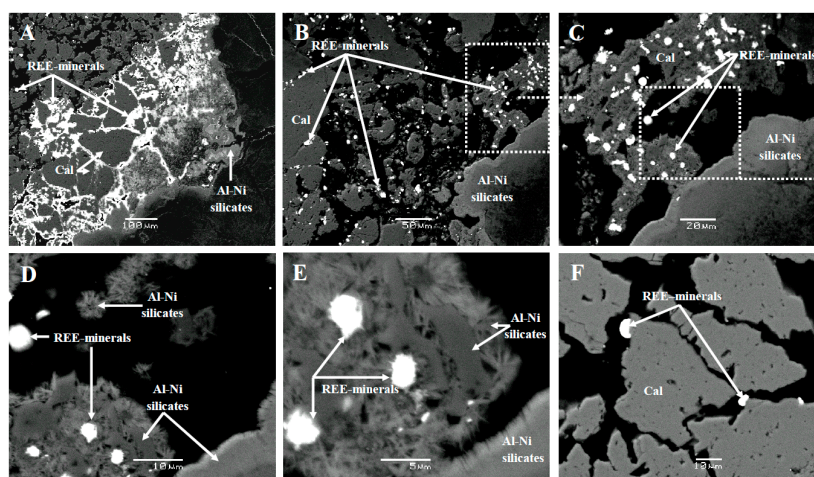


Figure 7. Representative back scattered images showing: Rare Earth Elements—minerals (white) associated with calcite (A–C,F) and Al–Ni–silicates (B–E) in the NB group of samples from the contact between the lowermost part of the bauxite laterite ore and the carbonate basement.

Raman spectroscopy was additionally employed to investigate the REE-minerals from the studied profile. Representative Raman spectra of the REE-carbonates, studied herein, are given in Figure 8. They refer to the bastnaesite group minerals and exhibit three distinguished Raman features: (Figure 8a) Raman spectra with dominant bands at around 795, 776 and 202 cm^{-1} and minor ones at around 1350 and 1290 cm^{-1} (e.g., spectrum nissi 1_8); (Figure 8b) Raman spectra characterized by intense Raman bands at around 1086, 796, 783 and 768 cm^{-1} and minor ones at around 1530, 1336, 965, 748, 283, 253 and 195 cm^{-1} (e.g., spectrum nissi 1_1); and (Figure 8c) Raman spectra with main Raman bands arising at around 1086, 712 and 281 cm^{-1} (e.g., spectrum nissi 1_12).

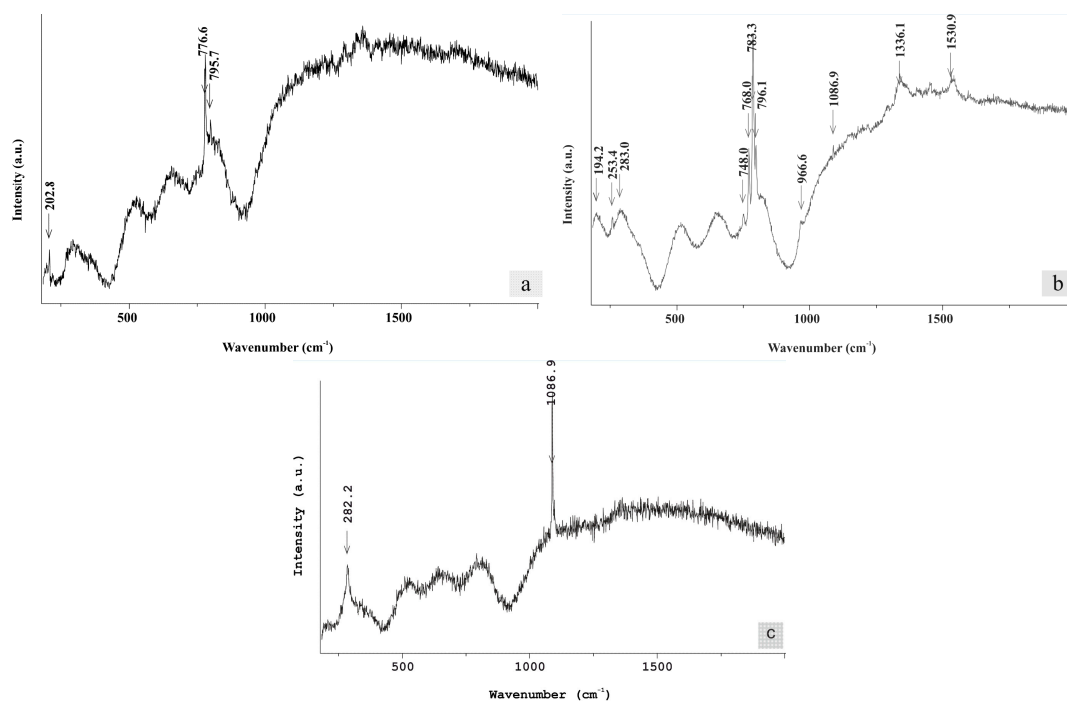


Figure 8. Representative Raman spectra of REE-bearing carbonates with dominant bands at around: (a) 795, 776 and 202 cm^{-1} ; (b) 1086, 796, 783 and 768 cm^{-1} ; and (c) 1086 and 282 cm^{-1} .

The Raman spectrum of bastnaesite/hydroxylbastnaesite has been reported to exhibit significant variations based on its chemical composition. A single intense band due to the symmetric stretching vibration (ν_1) of the carbonate groups appears at 1085 cm^{-1} for Canada bastnaesite-(Ce,La), at 1095 cm^{-1} for Pakistan bastnaesite-(Ce,La), at 1096 cm^{-1} for Norway bastnaesite-(Y,La) and at 965 cm^{-1} for Malawi hydroxylbastnaesite-(Ce,La) [21]; the latter remains controversial as it has been attributed either to carbonate bending mode [22] or to the OH deformation mode of hydroxylbastnaesite [21] and it is absent in the Raman spectra of any other halogenated carbonate. The variation of the ν_1 band position is a function of the chemical composition of the mineral. Fundamentally, the higher the ionic radius the lower the wavenumber of the symmetric stretching mode. Raman modes around the 700 cm^{-1} region are due to the in-plane bending mode (ν_4). As the carbonate groups become distorted from regular planar symmetry, this mode splits into two components. In bastnaesite, the variation in the position of the ν_4 band, usually observed at 729 cm^{-1} , reflects its composition. Two bands are observed for hydroxylbastnaesite at 602 and 569 cm^{-1} probably ascribed to the ν_4 mode [23].

Taking into consideration the afore-mentioned studies, we could come to the following band assignments:

- The Raman bands at 795 and 776 cm^{-1} in (Figure 8a), at 796 , 783 and 768 cm^{-1} in (Figure 8b) and at 712 cm^{-1} in (Figure 8c), are assigned to in-plane bending mode (ν_4) of the carbonate groups.
- The Raman band at 1086 cm^{-1} that is very dominant in (Figure 8c) and of lower intensity in the spectra of (Figure 8b) is assigned to the symmetric stretching vibration (ν_1) of the carbonate groups.
- The weak Raman band at around 965 cm^{-1} could be rather assigned to the OH^- deformation mode.

The shifts of the Raman band observed in this study compared to the published ones are considered to relate to their chemical composition, i.e., to the presence of Nd instead of Ce in the chemical composition of the carbonates studied herein, as well as to the presence of a considerable amount of Ca.

6. Discussion

In a global scale, the large REE deposits are associated with carbonatites and alkaline-peralkaline igneous rocks and hydrothermally altered silicate rocks, including pegmatites; on the contrary, REE concentrations by metamorphic or diagenetic processes are low ([6,14,24–26] and references therein). Fluorocarbonates, phosphates, silicates and oxides occur as disseminated and very fine-grained REE-minerals hosted by peralkaline felsic volcanic/volcaniclastic rocks. The bastnaesite-group minerals are among the most economically important ones, whereas their origin is related to late stages of magma evolution [26].

Fluorocarbonates in the Nissi (Patitira) bauxite laterite deposit, Lokris, are related with the lateritic weathering, which is an important process in the REE-enrichment in laterites [3–16,24]. The mineralogy of the weathered rocks and the physico/chemical conditions (temperature, acidity, redox potential) are among major controlling factors of the composition of the aqueous phase, which in turn can control the degree to which REEs are released to the downward moving fluids in contrast to iron that is quite reactive [3–16,24–26]. Multistage mineral phase deposition and transformations in the Lokris karst-type laterites is apparent (Figure 4; [3–16]). The epigenetic mobilization of Fe, Mn, Ni, Co and rare earth elements (REE) under reducing (due to the decomposition of organic material) and acidic (due to the decomposition of pyrite) conditions and subsequently re-deposition under alkaline conditions, during a diagenetic-post diagenetic stage at the Nissi (Lokris) laterite deposits, has been well established [3–16,27].

Experimental data on the Fe-(oxyhydr)oxides hematite, goethite, lepidocrocite and ferrihydrite suggest that Al-substitution in these materials may influence particle stability and phase transformation behavior, typically stabilizing the oxyhydroxide phases relative to the oxide one (hematite).

Lower Al-substitution energies for the oxyhydroxides goethite, lepidocrocite and ferrihydrite indicate that Al-substitution in these minerals might be more readily accomplished in a mixed-Al/Fe precipitation environment than for the oxide, hematite [28]. The presence of significant organic matter and Fe–Al–(oxyhydr)oxides may suggest that subsequent to the deposition of varying forms of pyrite [16], the deposition of goethite and Al-hydroxides, co-existing and/or cross-cutting earlier goethite and matrix, took place. Besides, goethite replacing pyrite (Figure 5B) and exhibiting elevated contents of aluminum and arsenic (Table 4), may be related with sorption and replacement processes, due to the metastable oxyhydroxide ferrihydrite with respect to goethite, since nanoparticulate under typical surface conditions, has high specific surface area and significant reactivity toward the sorption of aqueous contaminants (AsO_4^{3-} , SO_4^{2-} , among others [29]). In addition, the negative Gibbs free energy (ΔG°) values for arsenite and arsenate sorption on Fe-rich soil concretions are consistent with spontaneous reaction between the species and the medium [29].

There is a debate on whether the mineral is of direct organic or inorganic origin [30–39]. The relatively high content of organic matter (Tables 2 and 3), the SEM images, resembling bacteriomorphic goethite (Figure 5) coupled with the negative $\delta^{34}\text{S}$ values for sulfide-bearing samples from the Nissi area [16] may suggest the existence of the appropriate conditions for element bio-leaching and bio-mineralization. However, the detection of molecular and elemental bio-signatures regarding bacteriomorphic goethite requires furthermore research. Employing additional techniques, such as a mass spectrometry (MS, based on laser or ion-beams), in microscale and/or in nanoscale, is amongst our interests for future research.

Bastnaesite series can be classified into four types based on the predominant rare earth element [40,41]: bastnaesite-(Ce), [(Ce,La) CO_3 ,F], bastnaesite-(La), [(La,Ce) CO_3 ,F], bastnaesite-(Y), [(Y,Ce) CO_3 ,F] and bastnaesite-(Nd). The most frequent REE minerals in karstic deposits are members of the bastnaesite group, including: Synchysite-(Nd), bastnaesite-(Ce) and bastnaesite-(Nd), hydroxylbastnaesite-(Nd,La) and hydroxylcarbonate-(Nd,La). The occurrence of REE-phosphates and alkaline earth phosphates, such as monazite-(Nd), monazite-(La) and neodymian goyasite is relatively rare [14,27]. The REE minerals as identified by previous authors at the Nissi laterite deposits have been described within black Mn-oxide assemblages and are dominated by bastnaesite, hydroxylcarbonate-(Nd,La) and hydroxylbastnaesite-(Nd,La) [7,10].

In addition to REE-minerals described by above authors, a predominance of La (average 23 wt % La_2O_3) over Ce (0–2 wt % CeO_2) and the presence of Pr (average 5 wt % Pr_2O_3), Nd (average 23 wt % Nd_2O_3), Y (3–6 wt % Y_2O_3) and F (4–8 wt % F) in REE-minerals presented (Figure 7; Table 6) suggests that the investigated bastnaesites differ compared to those described by previous authors in terms of:

- (a) Their chemical composition compared to the hydroxylbastnaesite described at the Nissi deposits. Ideal bastnaesite simplified and calculated as LaCO_3F [42] contains ~8% F. Since Table 6 presents two data with >5% F these are not hydroxyl bastnaesite, but normal (fluorine) bastnaesite, although analysis in column 2 could be the OH variant.
- (b) Their association with margins of calcite grains (Figure 7F) and its intergrowths with Al–Ni–silicates (Figure 7B–E).

The latter texture relationships, combined with the major negative Ce-anomaly in the corresponding REE-patterns (Figure 4a), may indicate a late stage deposition of the investigated bastnaesites under reducing alkaline conditions. In contrast the Ce-positive anomaly in the uppermost part of the profile II (Figures 2 and 4a) may reflect the oxidation of Ce^{3+} to Ce^{4+} and its incorporation in other Ce-rich minerals.

Table 4. Representative SEM-EDS analyses of Fe-Al (hydroxyl) oxides from bauxite laterite (Profile I, Samples P1.2–P3.2, Figure 5).

wt %	Hematite	Hematite	Hematite	Goethite	Goethite	Goethite	Goethite	Goethite Bacteriomorphic	Boehmite	Boehmite
SiO ₂	2.8	4.1	2.6	4.6	3.0	4.4	8.9	9.8	0.3	0.8
Fe ₂ O ₃	85.6	84.4	87.4	79.5	78.6	79.4	67.2	60.3	1.8	0.9
Al ₂ O ₃	2.6	2.4	4.6	5.7	4.0	5.7	8.5	10.0	81.7	84.1
Cr ₂ O ₃	0.9	0.6	0.8	n.d.	n.d.	n.d.	0.3	0.4	n.d.	n.d.
MgO	n.d.	n.d.	n.d.	n.d.	n.d.	n.d.	0.7	2.3	n.d.	n.d.
CaO	n.d.	n.d.	n.d.	0.4	0.4	0.4	n.d.	0.4	n.d.	n.d.
TiO ₂	n.d.	n.d.	2.2	n.d.	0.3	n.d.	1.9	1.5	n.d.	0.4
MnO	0.4	0.6	n.d.	n.d.	n.d.	n.d.	0.4	0.4	n.d.	n.d.
NiO	n.d.	n.d.	0.7	n.d.	n.d.	n.d.	0.6	1.4	n.d.	n.d.
As ₂ O ₃	n.d.	n.d.	n.d.	n.d.	n.d.	n.d.	1.2	1.6	0.8	n.d.
SO ₄	n.d.	0.4	n.d.							
Total	92.3	92.1	98.3	90.1	86.3	89.9	89.7	88.1	86.7	87.1

Table 5. X-ray powder diffraction data for Bastnaesite and Al–Ni–silicates from the Nissi (Patitira) bauxite laterite deposit. Data from [12] concerning “the unknown Al–Ni–silicate mineral” from the nearby Aghios Ioannis deposit, are given for comparison.

Bastnaesite				Takovite				“The Maksimovic Unknown Al–Ni Silicate Mineral”				
00-011-0340 (I)				00-015-0087 (N)				Present Study		Data from Maksimovic 2003		
<i>hkl</i>	<i>I/I</i> ₀	<i>d</i> _{obs}	<i>d</i> _{calc}	<i>hkl</i>	<i>I/I</i> ₀	<i>d</i> _{obs}	<i>d</i> _{calc}	<i>d</i> _{obs}	<i>hkl</i>	<i>I/I</i> ₀	<i>d</i> _{obs}	<i>d</i> _{calc}
002	40	4.881	4.880	001	100	7.54	7.57	11.8	002	48	11.650	11.718
110	70	3.564	3.564	002	90	3.77	3.77	5.90	004	3	5.857	5.859
112	100	2.878	2.879	003	90	2.554	2.552	3.94	−106	100	3.935	3.933
004	9	2.445	2.445	-	80	2.267	2.264	2.575	108	100	2.563	2.565
302	40	1.897	1.898	-	20	2.036	2.031	2.443	032	3	2.444	2.442
220	9	1.783	1.783	004	90	1.921	1.917	1.503	−3115	27	1.503	1.503
006	1	1.629	1.629	005	80	1.513	1.510	-	-	-	-	-
304	15	1.572	1.573	-	80	1.447	1.481	-	-	-	-	-
116	9	1.480	1.481	-	-	-	-	-	-	-	-	-
224	11	1.439	1.439	-	-	-	-	-	-	-	-	-

Symbols: *I*: Intensity, *I*₀: Maximum Intensity, *I/I*₀ (×10): Relative Intensity, *d*: d-spacing, *d*_{obs}: d observed, *d*_{calc}: d calculated. “*hkl*” is Miller indices.

Table 6. Representative scanning electron microscope-energy dispersive spectroscopy (SEM-EDS) analyses of authigenic REE minerals from the Nissi (Patitira) bauxite laterite deposit. Data for 4, 5 from [10].

wt %	1	2	3	Hydroxylcarbonate ⁴	Hydroxylbastnaesite ⁵
SiO ₂	0.5	n.d.	0.5	-	-
CaO	6.4	8.0	5.9	0.1–6	1.6
MgO	n.d.	0.5	0.5	-	-
La ₂ O ₃	23.9	22.7	23.3	17.3–35.3	28.4
CeO ₂	n.d.	1.9	n.d.	-	-
Pr ₂ O ₃	5.0	4.6	5.2	7.0–9.1	6.1
Nd ₂ O ₃	23.6	21.5	22.9	28.0–34.5	27.9
Sm ₂ O ₃	n.d.	n.d.	n.d.	2.8–6.1	3.9
Eu ₂ O ₃	n.d.	n.d.	n.d.	0.7–1.5	1.1
Gd ₂ O ₃	n.d.	n.d.	2.3	1.2–2.5	2.8
Tb ₂ O ₃	n.d.	n.d.	n.d.	-	-
Dy ₂ O ₃	n.d.	n.d.	n.d.	0.2–0.7	1.3
Er ₂ O ₃	n.d.	n.d.	n.d.	0.10	0.7
Yb ₂ O ₃	n.d.	n.d.	n.d.	0.20	-
Y ₂ O ₃	5.7	5.2	2.37	0.1–0.6	2
SO ₄	0.7	0.7	n.d.	-	-
F	6.0	4.4	7.5	0.1–0.4	4
Total	71.8	69.5	70.3	-	79.8

Table 7. Representative SEM-EDS analyses of fine-grained intergrowths of Al–Ni–silicates and asbolane (Profile II, Samples NB, Figures 3 and 7).

wt %	Asbolane				Al–Ni–Silicates				
SiO ₂	28.4	21.9	11.1	1.8	24.4	21.4	22.1	35.9	37.3
Al ₂ O ₃	29.5	22.3	16.4	9.4	26.4	23.5	27.4	33.6	32.9
CaO	1.9	1.8	1.1	n.d.	n.d.	n.d.	n.d.	0.6	2.6
TiO ₂	n.d.	n.d.	n.d.	n.d.	n.d.	n.d.	n.d.	n.d.	n.d.
MnO	7.1	10.9	19.6	27.2	n.d.	n.d.	n.d.	n.d.	n.d.
FeO	0.4	n.d.	3.4	2.5	n.d.	n.d.	n.d.	n.d.	n.d.
NiO	6.3	7.5	15.7	17.9	32.8	26.6	25.1	3.4	n.d.
CoO	7.4	8.1	12.8	14.6	n.d.	n.d.	n.d.	n.d.	n.d.
SO ₄	n.d.	0.5	n.d.	0.4	1.8	2.0	n.d.	n.d.	n.d.
Total	81.0	73.4	80.1	73.8	85.3	73.50	74.6	73.5	72.8

According to the literature, bastnaesite (CeFCO₃), synchysite (CeFCO₃·CaCO₃), parisite (2CeFCO₃·CaCO₃), and roentgenite (3CeFCO₃·2CaCO₃) belong to the REE fluorocarbonate group known as the bastnaesite series ([43] and references therein). The bastnaesite mineral group presents two common features: (i) the structure can be broadly described as the stacking of three types of layers (CeF, CO₃ and Ca) along the *c*-axis; and (ii) the Ce/F ratio in all the phases is 1, indicating that this feature is common in all members of the group. Thus, these minerals differ in the orientation of carbonate ion within the carbonate layers, the order of staking of the different type of layers and the length of the crystallographic *c*-axis. Commonly, fluorocarbonates are polycrystals with syntaxial intergrowth of two species in contact along an irregular surface or along repeated parallel planes (0001). The *a*-axes of the two species may have the same or opposite directions. In the latter case, the two species are related to each other as two individual twins with a rotation of 60° around the *c* ternary axis. All pairs have been observed, except the bastnaesite-synchysite pair [43].

The syntactic intergrowths can be described as mixtures of bastnaesite and synchysite. Manfredi et al. [43] considered bastnaesite-(Ce) and synchysite-(Ce) as two end-members and that parisite and roentgenite are ordered mixtures of bastnaesite (B) and synchysite (S) in single layers stacked along the *c* crystallographic axis direction. Parisite can be considered a BS stacking and roentgenite a BS2 stacking [43] and references therein.

Minerals of this series are often affected by stacking faults, disorder of chemical composition, superstructures, twinning, polytypism and syntactic intergrowths during the course of crystallization and crystal growth along with other mineral phases, making it difficult to obtain crystallographic data on the one structures of the minerals [44].

Additionally, crystal structures of these minerals tend to have a layered topology. The planar carbonate groups are inclined (standing on-edge) with respect to the overall structural layering. The addition of another anion, F^- , can influence this topology. The development of a structural hierarchy of fluoride carbonates requires consideration of ratios of these two anions and their attached cationic polyhedral groups [45].

According to Grice et al. [45], as a consequence of the presence of similar rare earth fluoride carbonate layers, twinning is frequently observed, together with syntactic intergrowth. All associations of the above minerals exist and were early recognized from morphological measurements. These features also explain the very long resistance of these minerals toward accurate structure determinations [45].

In present study, the XRD pattern shows reflections assigned to bastnaesite. The observed high contents of Ca (CaO from 6.37 wt % to 8.04 wt %, Table 6) in REE-minerals presented indicate that they are not pure bastnaesites and that probably is a case of syntactic intergrowth of parisite with bastnaesite, synchysite or roentgenite, which is typical for these minerals.

The poor quality exhibiting by the powder X-ray diffraction pattern concerning the fluorocarbonate minerals (Figure 6), is probably due to:

- (a) lattice deformation or disordering as a result of substitutions of Ce or La by Nd and of Ce by Y;
- (b) poor crystallization of the mineral;
- (c) very small size of the mineral crystallites; and
- (d) syntactic intergrowth that may occur.

For the clarification of the minerals and structural features of the studied phases, additional techniques (such as high-resolution transmission electron microscopy (HRTEM)), should be conducted and this subject is amongst our interests for further research.

On the Origin of REE Fluorocarbonate Minerals

Parent rocks of the Ni-Fe deposits in the Lokris area, are primarily harzburgites, which represent the erosional outliers of a probable “complete” ophiolitic nappe that were transformed to serpentinites. Within the serpentine bodies of the basal tectonic mélangé, xenoliths of basic and sedimentary rocks are included, while a continuous transition from karstic Ni-Fe deposits towards bauxite material in a southern direction has been reported [4,6,7].

Although the REE content in ultramafic rocks is usually very low, there is a significant REE content along with other metals such as Al, Fe, Mn, Ni contents in mafic rocks and serpentinites parent rocks [6,7] suggesting that the ophiolitic rocks cannot be precluded as a REE source. Recently, a review of the regularities of REE distribution in minerals contained in mafic and ultramafic rocks as accessory phases was performed [46]. These minerals include garnets, zircons, apatites and perovskites, which can accumulate high concentrations of REE in their structure, as well as chrome spinels, ilmenites, and micas which can accumulate, only limited contents of these trace elements [46]. In addition, the Europium in other samples (Table 6) is not depleted relative to neighboring REE (Sm and Gd) in the bulk ores, suggesting an original mantle source for the REE, since crustal rocks are mostly Eu-negative. In addition, the apparent Yttrium enrichment (Table 6) is consistent with the USGS model of origin from ultramafic rocks [47] including along contacts between ultramafic rocks and carbonate rocks.

However, mineralogical characteristics, in particular the occurrence of different morphological forms of goethite (Figure 5) of varying composition (Table 4), with inclusions of chromite (Figure 5A) inherited from different sources [1] point to a dynamic cycling of the parent material. The occurrence of the above rare earth minerals described herein and by previous authors, all in the lowermost

part of laterite ores at their contact with the carbonate basement may suggest small differences in the conditions during their precipitation and/or variations in the REE source. In addition to the weathering process the studied profiles as allochthonous laterites lying on a carbonate basement, with well-established characteristics of a multistage re-mobilization and re-deposition [3–6,13,48] may have been affected by other processes.

The extensive presence of total organic matter (O.M.) at the contact of the Nissi (Patitira) bauxite laterites and the carbonate basement (Table 2; [16]) appears to create the appropriate conditions for iron and REE leaching and re-deposition [20,33,49–55]. The preferential occurrence of REE-minerals in the lower transitional zone and within the underlain limestone (Figure 7) itself suggests that their formation was controlled by physico-chemical conditions, such as an alkaline barrier, redox potential, solubility, supersaturation [29,56] rather than by the precursor rocks. The presence of rare earth minerals between calcite crystals (Figure 7) probably indicates late stage deposition under reducing alkaline conditions.

The enrichment of the REE at the Nissi (Patitira) concentrated in bastnaesite-group minerals is thought to have been caused by long-term leaching and re-deposition on karstified limestone, during a subsequent stage under alkaline conditions [10,24,29]. Although the dominant oxidation state of the REE in aqueous solution at 25 °C is the 3+ state, Ce behaves differently from the rest of the REE, due to the possibility of being oxidized from Ce³⁺ to Ce⁴⁺ in a relatively strong oxidizing environment [8,40,57]. Therefore the positive cerium anomalies occurring in the upper parts of the Nissi profile, and the negative one at the lowest part of the deposit, in contrast to the rest of the REE transported downward, are probably due to the difference in the breakdown of REE-bearing minerals under similar physico/chemical conditions. With respect to the fluorine source, the highest fluorine contents (up to 1200 ppm) that have been recorded in mafic rocks [58] and the presence of fluor-apatite in ophiolitic mafic rock [59,60], suggest a contribution of F-bearing minerals in laterites associated the weathering of such country rocks. In addition, the presence of fluor-hydroxyl-apatite in Fe-Ni-laterites of northern Greece, either as a clastic and/or authigenic mineral, coupled with its texture feature, showing gradual dissolution of apatite crystals [60] may indicate that apatite dispersed throughout the upper parts of the Nissi (Patitira) laterite deposit was unstable during an epigenetic stage. Fluorine is slightly mobile, under natural soil conditions, but in acid soils its solubility increases [58], following probably the mobilization of REE.

Since precipitation of REE-hydroxides markedly decreases from La to Lu, from pH 8.4 to 6.0, the REE plots showing a negative slope for samples at the footwall limestone (Figure 4a) confirm the importance of the pH for the fractionation of REE in the sedimentary cycle. More specifically, in a karstic environment, where the water is weakly alkaline to alkaline, the argillaceous material collected in depressions will be enriched in light REE (LREE) whereas heavy REE (HREE) will mostly be removed by solutions, through different channels in karst [61,62]. The compositional variability of all authigenic REE minerals in karstic deposits has been well established [14] and it is caused basically by two types of substitution: Nd and La, but more frequently Nd, can substitute for Ce, forming Nd- or La-dominant minerals, and OH ions can substitute for F in the structure of bastnaesite, forming hydroxylbastnaesites ([14] and references therein).

Although the factors controlling REE-stability on molecular scale are still unclear, the stability of the described (La,Nd,Y)(CO₃)F member of the bastnaesite-group and the associated minerals in the Nissi (Patitira) deposit may point to the significant role of the redox and pH conditions during mobilization and re-precipitation processes caused Fe-leaching and residual Al-enrichment at the top of the deposit (Figure 2B).

7. Conclusions

Combining mineralogical and geochemical data presented in this study and current literature knowledge allow us to make the following conclusions:

- In addition to the hydroxylbastnaesites described by previous authors in the Nissi (Patitira) laterite deposit, a (La,Nd,Y)(CO₃)F member of the bastnaesite group, associated with Al–Ni–silicates, was identified.
- The enrichment of the REE at the Nissi (Patitira) concentrated in bastnaesite-group minerals, the intergrowths between REE-minerals and Al–Ni–silicates and their association with goethite microtextures interpreted as bacteriomorphic support the remobilization of REE along with iron downward and re-precipitation on karstified limestone.
- The stability of the (La,Nd,Y)(CO₃)F may reflect this dependence on the source rocks and the local variations of pH-Eh.

Acknowledgments: The National and Kapodistrian University of Athens (NKUA) is greatly acknowledged for the financial support (Grant No. KE_11078) of this work. Evaggelos Michailidis is thanked for his assistance with the probe analyses. The authors would also like to thank GMM LARCO SA for their permission to collect samples from the Nissi area deposits of the Aghios Ioannis mines.

Author Contributions: Sofia Kalatha and Maria Economou-Eliopoulos collected the samples, provided the field information and performed all types of analyses. Maria Perraki performed and interpreted the Raman data. The X-ray powder diffraction (XRD) data were obtained and interpreted by Ioannis Mitsis. All authors contributed to the elaboration and interpretation of the data and to the final revision of the manuscript.

Conflicts of Interest: The authors declare no conflict of interest.

References

1. Eliopoulos, D.G.; Economou-Eliopoulos, M.; Apostolikas, A.; Golightly, J.P. Geochemical features of nickel–laterite deposits from the Balkan Peninsula and Gordes, Turkey: The genetic and environmental significance of arsenic. *Ore Geol. Rev.* **2012**, *48*, 413–427. [[CrossRef](#)]
2. Baker, J.; Cassard, D.; Grundfelt, B.; Ehinger, S.; D’Hugues, P.; Gaál, G.; Kaija, J.; Kurylak, W.; Mizera, W.; Sarlin, J.; et al. A New Approach to Mineral Resources in Europe—ProMine. In Proceedings of the Sustainable Production and Consumption of Mineral Resources—Integrating the EU’s Social Agenda and Resource Efficiency, Wroclaw, Poland, 20–22 October 2011.
3. Eliopoulos, D.; Economou-Eliopoulos, M. Geochemical and mineralogical characteristics of Fe–Ni and bauxite–laterite deposits of Greece. *Ore Geol. Rev.* **2000**, *16*, 41–58. [[CrossRef](#)]
4. Alevizos, G. Mineralogy, Geochemistry and Origin of the Sedimentary Fe–Ni Ores of Lokris. Ph.D. Thesis, Technical University of Crete, Chania, Greece, 1997; p. 245.
5. Albandakis, N.D. The nickel-bearing iron-ores in Greece. In Proceedings of the International Symposium on Metallogeny of Mafic Ultramafic Complexes, Athens, Greece, 9–11 October 1980; UNESCO IGCP-169; National Technical University of Athens: Athens, Greece, 1980; pp. 194–213.
6. Valetton, I.; Biermann, M.; Reche, R.; Rosenberg, F. Genesis of Nickel laterites and bauxites in Greece during the Jurassic and Cretaceous, and their relation to ultrabasic parent rocks. *Ore Geol. Rev.* **1987**, *2*, 359–404. [[CrossRef](#)]
7. Rosenberg, F. Geochemie und Mineralogie lateritischer Nickel und Eisenerze in Lokris und auf Euböa, Griechenland. Ph.D. Thesis, University of Hamburg, Hamburg, Germany, 1984; p. 169.
8. Maksimovic, Z.; Skarpelis, N.; Panto, G. Mineralogy and geochemistry of the rare earth elements in the karstic nickel deposit of Lokris area, Greece. *Acta Geol. Hung.* **1993**, *36*, 331–342.
9. Economou-Eliopoulos, M.; Eliopoulos, D.G.; Apostolikas, A.; Maglaras, K. Precious and rare earth element distribution in Ni-laterite deposits from Lokris area, Central Greece. In Proceedings of the Fourth Biennial SGA Meeting, Turku, Finland, 11–13 August 1997; pp. 411–413.
10. Pantó, G.; Maksimovic, Z. Two new rare earth minerals in an unusual mineralization of the Nissi bauxite deposit, Greece. *Acta Geol. Hung.* **2001**, *44*, 81–93.

11. Maksimovic, Z. Hydrous nickel-containing clay-like minerals in the karstic environment. In Proceedings of the 11th International Clay Conference, Ottawa, ON, Canada, 15–21 June 1997; Kodama, H., Mermut, A.R., Torrance, J.K., Eds.; pp. 647–652.
12. Maksimovic, Z.J. An unknown Ni-Al hydrosilicate. *Acta Geol. Hung.* **2003**, *46*, 313–320. [[CrossRef](#)]
13. Maksimovic, Z. Karstic nickel deposit in the village Ba, near Ljig, Western Serbia: Ni-bearing minerals and their genesis. *Bull. Acad. Serbe Sci. Arts* **2004**, *42*, 341–361.
14. Maksimovic, Z. Genesis of Mediterranean karstic bauxites and karstic nickel deposits. *Bull. Acad. Serbe Sci. Arts* **2010**, *46*, 1–27.
15. Skarpelis, N. Lateritization processes of ultramafic rocks in Cretaceous times: The fossil weathering crusts of mainland Greece. *J. Geochem. Explor.* **2006**, *88*, 325–328. [[CrossRef](#)]
16. Kalatha, S.; Economou-Eliopoulos, M. Framboidal pyrite and bacteriomorphic goethite at transitional zones between Fe–Ni–laterites and limestones: Evidence from Lokris, Greece. *Ore Geol. Rev.* **2015**, *65*, 413–425. [[CrossRef](#)]
17. Valero-Garcés, B.; Arenas, C.; Delgado-Huertas, A. Depositional environments of Quaternary lacustrine travertines and stromatolites from high altitude Andean lakes, northwestern Argentina. *Can. J. Earth Sci.* **2001**, *38*, 1263–1283. [[CrossRef](#)]
18. Antoniadou, P.A.; Vgenopoulos, A.G. Study of the nickeliferous bauxite laterite in north of Kokkino area, Lokris. *Met. Min. Ann.* **1987**, *65*, 51–60.
19. ASTM. *Standard Test Methods for Moisture, Ash and Organic Matter of Peat and Other Organic Soils, Method D 2974-00*; American Society for Testing and Materials: West Conshohocken, PA, USA, 2000.
20. Laskou, M.; Economou-Eliopoulos, M. Bio-mineralization and potential biogeochemical processes in bauxite deposits: Genetic and ore quality significance. *Miner. Petrol.* **2000**, *107*, 471–486. [[CrossRef](#)]
21. Frost, R.L.; Dickfos, M.J. Raman spectroscopy of halogen-containing carbonates. *J. Raman Spectrosc.* **2007**, *38*, 1516–1522. [[CrossRef](#)]
22. Hong, W.; He, S.; Huang, S.; Wang, Y.; Hou, H.; Zhu, X. A Raman spectral studies of rare-earth (REE) fluoro-carbonate minerals. *Guangpuxue Yu Guangpu Fenxi* **1999**, *19*, 546–549.
23. Frost, R.L.; Palmer, S.J. Raman spectrum of decrespignyite [(Y,REE)₄Cu(CO₃)₄Cl(OH)₅·2H₂O] and its relation with those of other halogenated carbonates including bastnasite, hydroxybastnasite, parisite and northupite. *J. Raman Spectrosc.* **2011**, *42*, 2042–2048. [[CrossRef](#)]
24. Goodenough, K.M.; Schilling, J.; Jonsson, E.; Kalvig, P.; Charles, N.; Tuduri, J.; Dedy, E.A.; Sadeghi, M.; Schiellerup, H.; Muller, A.; et al. Europe's rare earth element resource potential: An overview of REE metallogenetic provinces and their geodynamic setting. *Ore Geol. Rev.* **2016**, *72*, 838–856.
25. Verplanck, P.L.; Mariano, A.N.; Mariano, A., Jr. (Eds.) Rare Earth Element Ore Geology of Carbonatites. In *Reviews in Economic Geology*; SEG: Littleton, CO, USA, 2016; Chapter 1; pp. 1–5.
26. Dostal, J. Rare Metal Deposits Associated with Alkaline/Peralkaline Igneous Rocks. In *Reviews in Economic Geology*; Verplanck, P.L., Hitzman, M.W., Eds.; SEG: Littleton, CO, USA, 2016; Chapter 2; pp. 6–33.
27. Maksimovic, Z.J.; Pantó, G. Authigenic rare earth minerals in karst-bauxites and karstic nickel deposits. In *Rare Earth Minerals, Chemistry, Origin and Ore Deposits*; Jones, A.P., Wall, F., Williams, C.T., Eds.; Springer: Berlin, Germany, 1996; Chapter 10; pp. 257–279.
28. Pinney, N.; Morgan, D. Thermodynamics of Al-substitution in Fe-oxyhydroxides. *Geochim. Cosmochim. Acta* **2013**, *120*, 513–530. [[CrossRef](#)]
29. Navrotsky, A.; Mazeina, L.; Majzlan, J. Size-driven structural and thermodynamic complexity in iron oxides. *Science* **2008**, *319*, 1635–1638. [[CrossRef](#)] [[PubMed](#)]
30. Donald, R.; Southam, G. Low temperature anaerobic bacterial diagenesis of ferrous monosulfide to pyrite. *Geochim. Cosmochim. Acta* **1999**, *63*, 2019–2023. [[CrossRef](#)]
31. Folk, R.L. Nannobacteria and the formation of framboidal pyrite: Textural evidence. *Int. J. Earth Syst. Sci.* **2005**, *114*, 369–374. [[CrossRef](#)]
32. Heim, C. An Integrated Approach to the Study of Biosignatures in Mineralizing Biofilms and Microbial Mats. Ph.D. Thesis, University of Göttingen, Göttingen, Germany, 2010; p. 175.
33. Kock, D.; Schippers, A. Geomicrobiological investigation of two different mine waste tailings generating acid mine drainage. *Hydrometallurgy* **2006**, *83*, 167–175. [[CrossRef](#)]
34. Love, L.G. Micro-organisms and the presence of syngenetic pyrite. *Q. J. Geol. Soc. Lond.* **1957**, *113*, 429–440. [[CrossRef](#)]

35. Love, L.G.; Amstutz, G.C. Review of microscopic pyrite from the Devonian Chattanooga Shale and Rammelsberg Banderz. *Fortschr. Mineral.* **1966**, *43*, 273–309.
36. Ohfuji, H.; Rickard, D. Experimental syntheses of framboids—A review. *Earth Sci. Rev.* **2005**, *71*, 147–170. [[CrossRef](#)]
37. Sand, W.; Gehrke, T.; Hallmann, R.; Schippers, A. Sulfur chemistry, biofilm and the indirect attack mechanism—A critical evaluation of bacterial leaching. *Appl. Microbiol. Biotechnol.* **1995**, *43*, 961–966. [[CrossRef](#)]
38. Schippers, A.; Jørgensen, B.B. Oxidation of pyrite and iron sulfide by manganese dioxide in marine sediment. *Geochim. Cosmochim. Acta* **2001**, *65*, 915–922. [[CrossRef](#)]
39. Wilkin, R.T.; Barnes, H.L. Formation processes of framboidal pyrite. *Geochim. Cosmochim. Acta* **1997**, *61*, 323–339. [[CrossRef](#)]
40. Gaines, R.V.; Skinner, H.C.W.; Foord, E.E.; Mason, B.; Rosenzweig, A. *Dana's New Minerals*, 8th ed.; John Wiley and Sons, Inc.: New York, NY, USA, 1997.
41. Miyawaki, R.; Yokouama, K.; Husdal, T. Bastnaesite-(Nd), a new Nd-dominant member of the bastnaesite group from the Stetind pegmatite, Tysfjord, Nordland, Norway. *Eur. J. Miner.* **2013**, *25*, 187–191. [[CrossRef](#)]
42. Jones, A.P.; Wyllie, P.J. Solubility of rare earth elements in carbonatite magmas, indicated by the liquidus surface in CaCO₃-Ca(OH)₂-La(OH)₃ at 1 kbar pressure. *Appl. Geochem.* **1986**, *1*, 95–102. [[CrossRef](#)]
43. Manfredi, T.R.; Bastos Neto, A.C.; Pereira, V.P.; Barbanson, L.; Schuck, C. The parisite-(Ce) mineralization associated with the Fazenda Varela carbonatite (Correia Pinto, SC). *Pesquisas em Geociências* **2013**, *40*, 295–307.
44. Meng, D.; Wu, X.; Han, Y.; Meng, X. Polyttypism and microstructures of the mixed-layer member B2S, CaCe₃(CO₃)₄F₃ in the bastnaesite-(Ce)-Synchysite-(Ce) series. *Earth Planet. Sci. Lett.* **2002**, *203*, 817–828. [[CrossRef](#)]
45. Grice, J.D.; Maisonneuve, V.; Leblanc, M. Natural and Synthetic Fluoride Carbonates. *Chem. Rev.* **2007**, *107*, 114–132. [[CrossRef](#)] [[PubMed](#)]
46. Lesnov, F.P. Consistent patterns of rare earth element distribution in accessory minerals from rocks of mafic-ultramafic complexes. *Cent. Eur. J. Geosci.* **2013**, *5*, 112–173. [[CrossRef](#)]
47. Marsh, E.E.; Anderson, E.D. *Ni-Co Laterite Deposits: U.S. Geological Survey*; Open-File Report 2011-1259; U.S. Geological Survey: Reston, VA, USA, 2011; p. 9.
48. Skarpelis, N.; Perlikos, P.; Gale, N.; Stos-Gale, S. Rare earth elements and gold in laterite derived sedimentary nickeliferous iron ores: The Marmeiko deposit, Beotia, continental Greece. *Bull. Geol. Soc. Greece* **1989**, *XXVI*, 121–128.
49. Silverman, S.R. Carbon isotopic evidence for the role of lipids in petroleum formation. *J. Am. Oil Chem. Soc.* **1967**, *44*, 691–695. [[CrossRef](#)]
50. Hiskey, J.B.; Schlitt, W.J. (Eds.) Aqueous oxidation of pyrite. In Proceedings of the Second SME-SPE International Solution Mining symposium, Denver, CO, USA, 18–20 November 1981; pp. 55–74.
51. Nowaczyk, K.; Juszczak, A.; Domka, F. Microbiological oxidation of the waste ferrous sulfate. *Pol. J. Environ. Stud.* **1999**, *8*, 409–416.
52. Southam, G.; Saunders, J. The geomicrobiology of ore deposits. *Econ. Geol.* **2005**, *100*, 1067–1084. [[CrossRef](#)]
53. Russell, M.J.; Hall, A.J.; Boyce, A.J.; Fallick, A.E. 100th Anniversary special paper: On hydrothermal convection systems and the emergence of life. *Econ. Geol.* **2005**, *100*, 419–438.
54. Stock, E.L. Minerals as energy sources for microorganisms. *Econ. Geol.* **2009**, *104*, 1235–1248.
55. Laskou, M.; Economou-Eliopoulos, M. The role of microorganisms on the mineralogical and geochemical characteristics of the Parnassos-Ghiona bauxite deposits, Greece. *J. Geochem. Explor.* **2007**, *93*, 67–77. [[CrossRef](#)]
56. Norton, S. Laterite and bauxite formation. *Econ. Geol.* **1973**, *63*, 353–361. [[CrossRef](#)]
57. Braun, J.-J.; Pagel, M.; Muller, J.-P.; Bilong, P.; Michard, A.; Guillet, B. Cerium anomalies in lateritic profiles. *Geochim. Cosmochim. Acta* **1990**, *54*, 781–795. [[CrossRef](#)]
58. Kabata-Pendias, A.; Pendias, H. *Trace Elements in Soils and Plants*; CRC Press: Boca Raton, FL, USA, 2001.
59. Mitsis, I.; Economou-Eliopoulos, M. Occurrence of apatite with magnetite in an ophiolite complex (Othrys), Greece. *Am. Miner.* **2001**, *86*, 1143–1150. [[CrossRef](#)]
60. Economou-Eliopoulos, M. Apatite and Mn, Zn, Co-enriched chromite in Ni-laterites of northern Greece and their genetic significance. *J. Geochem. Explor.* **2003**, *80*, 41–54. [[CrossRef](#)]

61. Ronov, A.B.; Balashov, Y.A.; Migdisov, A.A. Geochemistry of the rare earth in the sedimentary cycle. *Geochem. Int.* **1967**, *4*, 1–17.
62. Cullers, R.; Chandhuri, S.; Arnold, B.; Lee, M.; Wolf, C.W., Jr. Rare earth distribution in clay minerals and in the clay sized fraction of the Lower Permian Havensville Eskridge shales of Kansas and Oklahoma. *Geochim. Cosmochim. Acta* **1975**, *39*, 1691–1703. [[CrossRef](#)]



© 2017 by the authors. Licensee MDPI, Basel, Switzerland. This article is an open access article distributed under the terms and conditions of the Creative Commons Attribution (CC BY) license (<http://creativecommons.org/licenses/by/4.0/>).